Rail failure root cause analysis on North American Railway

Szablewski, Daniel; Caldwell, Robert

Publisher's version / Version de l'éditeur:

Canadian & Cold Regions Rail Research Conference 2021, pp. 56-63, 2021-11-09

Canadian & Cold Regions
Rail Research Conference
2021

Rail failure root cause analysis on North American railway

Daniel Szablewski and Robert Caldwell
National Research Council Canada Automotive and Surface Transportation,
Ottawa, ON, Canada

ABSTRACT

NRC analyzed a broken rail that occurred on a North American Railway in the springtime. The break took place in 115RE standard rail placed in the high rail position of a 5 degree lubricated curve. Rail inspection focused on verifying mechanical, microstructural and chemistry measurements against current AREMA guidelines for these material properties. In addition, fractography was carried out on the fracture surfaces that led to the critical rail failure.

The rail defect took place in heavily curved track territory. To pinpoint the root cause(s) of this failure NRC performed a site inspection on a 30 mile length of track inspecting 29 curves, observing running surface conditions, and recording rail profiles and eddy current measurements to build an understanding of track conditions that might have contributed to the observed critical rail failure.

The paper describes the methodology undertaken in this investigation and details the outcomes at each investigative step, along with conclusions shedding light on the impact of metrics on the critical rail defect that led to the train derailment. Emphasis is placed on overall running track conditions in the investigated subdivision and on factors affecting the derailment. The paper concludes with a list of recommendations on metrics that need to be monitored with greater scrutiny to prevent future derailments. Improved rail material selection and/or more stringent grinding maintenance practices are also suggested to help prevent rail defect occurrences that might lead to critical track failures in the future.

1 INTRODUCTION

Rail failures are a common occurrence in freight operations (TSBC, 2019). Operating conditions on these lines are such that rail is constantly placed in either the wear regime, where plastic deformation combines with natural wear to result in relatively rapid running surface profile deterioration or in the rolling contact fatigue (RCF) cracking regime, where RCF cracks at the running surface initiate as head checks that then progress to subsurface networks of interconnected cracks. Either of these damage mechanisms is detrimental to the rail life-cycle (Aquib Anis, 2018).

Established solutions address both the removal of pre-existing RCF cracks by grinding the rail at prescribed tonnage intervals to shapes that conform to the predominant wheel profile, and friction management through the gauge face/corner (GFC) lubrication of the high rail and top of rail friction modification (TOR FM) of both rails, to slow down rail wear and RCF progression (Wang et al., 2017; Harmon and Lewis, 2016).

Appropriate combination of these two solutions has been observed to extend the rail life (Tuzik, 2019). The ultimate goal of their application is to reach the ‘magic wear rate’ in the rail, wherein RCF crack growth occurs in step with rail wear, thereby minimizing the need for excessive grinding to target RCF removal and instead focus grinding effort on rail profile restoration (Magel et al., 2014).

At times preference is given to only one method (either lubrication or grinding), ignoring the need to apply both practices simultaneously to achieve the desired results. Lubrication is often applied intermittently (i.e. tanks are either not refilled regularly and/or dispensing bars are damaged preventing product from being delivered to the railhead) or grinding cycles are skipped (in favor of longer grinding intervals). Either of these actions creates an environment where rapid rail profile deterioration can take place and/or fatigue cracking in the rail can progress to form critical rail defects leading to derailments (Magel et al., 2016). The time interval to the appearance of critical rail defects usually varies according to track utilization (i.e. traffic frequency, tonnage accumulation), as well as which rail grade is being utilized, among others. Nevertheless, track integrity is decreased over time and often cannot be

reversed by 'catch-up' grinding if RCF progression into the rail is substantial (Sroba, 2003).

To make matters worse, the North American seasonal temperature swings that take place in Canada and northern USA act to increase stress on the rail network (CPR, 2019). In winter time cold temperatures increase rail tension that creates added tensile stress concentrations at the root tips of pre-existing RCF cracks. This condition can lead to rapid crack progression and rail critical failure.

National Research Council Canada (NRC) analyzed two such critical failures in ALGOMA C.C. 115RE 1985 standard rail. This paper addresses the findings from this investigation. In addition, a follow-up track inspection took place on the subdivision where the two critical failures occurred to observe 29 locations where potential future failures could develop. The methodology of selection criteria for these sites is described as well as the findings.

2 MATERIALS AND METHODS

The fractured rails taken out of service for defect root cause analysis had the following characteristics:

- ALGOMA C.C. 115RE 1985 standard rail
- High rail position in a 5.0 deg lubricated curve
- An approximate life-cycle tonnage of 130MGT
- Last grind cycles in 2005 (at 65MGT)
- Penny-sized fatigue cracks originating in high rails at the GFC in multiple locations (see Figure 1)

The laboratory metallurgical investigation consisted of the following analysis steps:

- Fractography of the broken rail section
- Analysis of the rail chemistry (per ASTM E1019-18, E1097-12, E1479-16)
- Analysis of the rail microcleanliness (per ASTM E3-11, E1245-03)
- Analysis of the rail mechanical properties:
    - Tensile testing (per ASTM E8-16a)
    - Fracture toughness testing (per ASTM E399-17) (PTS & MTS, 2021).

In addition, a site visit was arranged to a 30 mile stretch of track which included the locations of the rail fractures to measure and document the following high and low rail conditions:

- Dye penetrant of the rail running surface
- Crack depth measurements from the rail running surface using eddy current (EC)
- Transverse rail profile using Miniprof®
- Track gauge using track gauging bar
- Track superelevation using track gauging bar

The following section outlines the results of this analysis with contributing impacts on root causes.

3 RESULTS AND DISUSSION

3.1 Fractography of Broken Rail Sections

The broken rail pieces were scanned using portable eddy current (EC) technology to assess the depth of damage. In most locations, the crack depth from the running surface ranged from 4-5 mm. However, at the fractured location the fatigue cracks significantly exceeded those depth limits.

Both rail sections displayed significant wear and RCF cracks with intermittent spalling at both the GFC and TOR running surfaces. The wear was accompanied by signification plastic metal flow at the GFC, as evident by the formation of a plastic lip at the lower GFC. There was also significant field corner plastic flow on the TOR. In addition, there were no visible grinding marks that would indicated recent grinding on the running surface.

The rail sections had two main fracture zones. However, only one of these led to a critical rail failure that resulted in the train derailment. Both defects initiated at the GFC as fatigue cracks (indicated by yellow dotted zones in Figure 1). These fatigue cracks grew relatively slowly over time (as evidenced by fatigue growth rings). Once the remaining rail cross-section could no longer bear the load, critical failure took place. This critical failure was instantaneous, as evidenced by the fast brittle fracture of the remaining rail cross-section.

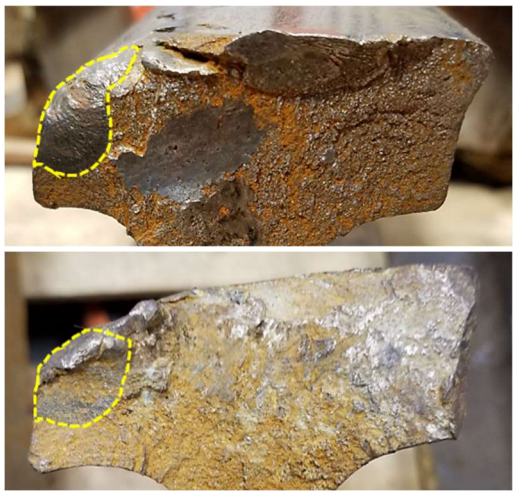

Figure 1. Examples of two (2) slow growth GFC fatigue defects (circled) that grew over time, which led to one of them causing the rail critical brittle failure.

During the track inspection portion of this work NRC took photographs and EC measurements of the scrapped rails which were still on site. This data was compared to the results acquired from the broken rail sections sent to NRC for analysis. The measured crack depths were in the same range (4-5 mm), with GFC damage being very similar to the one investigated at the NRC laboratory (see Figure 2).

Figure 2. Rail running surface condition of ALGOMA C.C. 115RE 1985 standard rail taken out of service at approximately 130MGT indicating severe GFC damage.

3.2 Rail Chemistry Test Results

Two rail chemistry samples were analyzed (i.e. samples 1C and 2C) to contrast their compositions against AREMA's current recommended standard rail chemistry values (AREMA, 2021). All tested elements were within the current guidelines (see Table 1).

Microstructural analysis of the fractured rail revealed it was nearly entirely pearlitic, with relatively minor amounts of ferrite at the grain boundaries. That was the expected microstructure from standard chemistry rail produced 30 years ago.

Table 1. Rail chemistry test results.

Chemistry Analysis
(per ASTM E1019-18, ASTM E1097-12 (reapproved 2017, modified), and ASTM E1479-16)

	Chemical Analysis Weight percent					
			AREMA recommended values for standard chemistry rail		Product Analysis, Weight Percent Allowance Beyond Limits of Specified Chemical Analysis	
Element	Chemistry Sample 1C	Chemistry Sample 2C	Minimum	Maximum	Under Minimum	Over Maximum
Carbon	0.73	0.73	0.74	0.86	0.04	0.04
Manganese	0.82	0.83	0.75	1.25	0.06	0.06
Phosphorus	0.015	0.015	-	0.020	-	0.008
Sulphur	0.023	0.023	-	0.020	-	0.008
Silicon	0.29	0.29	0.10	0.60	0.02	0.05
Chromium	0.01	0.01	-	0.30	-	-

3.3 Microcleanliness Test Results

Two rail microcleanliness samples were analyzed (i.e. samples 1MC and 2MC) to contrast their microstructures and reveal the presence of non-metallic inclusions. Both microstructures were found to be free of any voids and had a very low presence of oxides (see Table 2). The rail's microcleanliness values are in line with what is currently considered average in both intermediate and premium grades (see (Szablewski et al., 2011a; Szablewski et al., 2011b)).

Table 2. Rail microcleanliness test results.

Microcleanliness Test
(per ASTM E3-11 (reapproved 2017), and ASTM E1245-03 (reapproved 2016))

Element		Sample 1MC	Sample 2MC
Voids	Mean Volume %	0%	0%
	95% CI	N/A	N/A
	% RA	N/A	N/A
	Count/mm^2	0/mm^2	0/mm^2
Oxides	Mean Volume %	0.0054%	0.0034%
	95% CI	0.00058%	0.00031%
	% RA	11%	9.3%
	Count/mm^2	3/mm^2	2/mm^2
Mean Volume % (Voids + Oxides)		**0.0054%**	**0.0034%**
Maximum Volume % (Voids + Oxides)		**0.0292%**	**0.0089%**
Sulphides	Mean Volume %	0.040%	0.046%
	95% CI	0.0015%	0.0019%
	% RA	3.7%	4.2%
	Count/mm^2	30/mm^2	34/mm^2
	Maximum Volume %	**0.075%**	**0.080%**

3.4 Mechanical Test Results

Analysis of the rail's mechanical properties from two samples (i.e. sample 1T and 2T) indicated that yield strength (YS) and ultimate tensile strength (UTS) were below the current minimum AREMA recommended values (AREMA, 2021), see Table 3.

Table 3. Rail mechanical test results.

Tensile Test
(per ASTM E8-16a)

	Sample 1T	Sample 2T	minimum AREMA recommended values for standard chemistry
0.2% YS [ksi]	65.4	68.2	74.0
UTS [ksi]	129.7	129.4	142.5
Elong [%]	11	12	10

Fracture Toughness Test
(per ASTM E399-17)

	Sample 1F	Sample 2F
Kq [ksi(in)$^{1/2}$]	42.0	37.6

Lower YS values indicated that given the same stress level at the running surface, the tested rail was more prone to plastic flow than rail that meets the current minimum AREMA recommended YS values. In addition, lower UTS for the tested rail indicates that the maximum stress the rail had experienced in service before critical failure was lower than that for rail that meets AREMA's current minimum recommended UTS values.

The fracture toughness values (for samples 1F and 2F) were on the upper end of what is currently considered average in both intermediate and premium rail grades (see Table 3 and (Szablewski et al., 2011a; Szablewski et al., 2011b).

3.5 Track Inspection

A track inspection was carried out to better understand the rail running surface condition in a curve population representative of the entire subdivision. An analysis of the subdivision's track charts was carried out to select the representative curves. This work was done through the site selection criteria.

3.5.1 Curve Site Selection Criteria

During this portion of the work the main focus was to understand the distribution of curves on the subdivision and to develop a better knowledge of the potential problem size. The degree of track curvature and respective length vs. mile post (MP) for the entire subdivision were mapped out. This showed that all curves were in the 1-7 degree range (Figure 3), and that they were mostly below 1,200 feet in length (Figure 4).

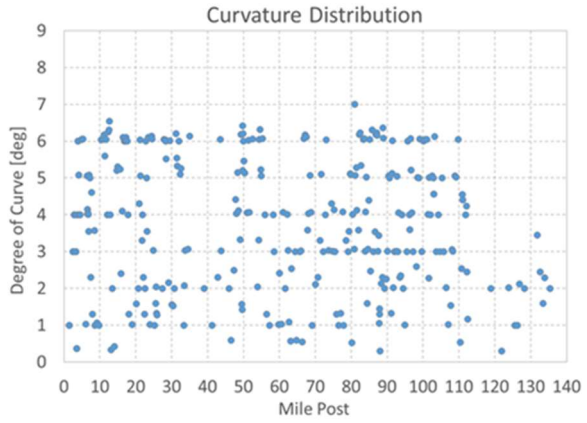

Figure 3. The degree of track curvature vs. mile post on the subdivision.

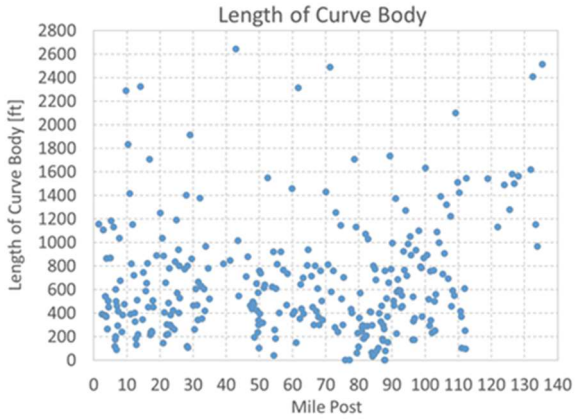

Figure 4. The length of each curve body vs. mile post on the subdivision.

NRC also mapped the posted train speed for all the curve locations (see Figure 5). Based on that data the maximum permissible train speed was 40 mph. However, this speed was the timetable speed of the train. Rail profile measurements would indicate whether trains operated predominantly above or below the balanced speed. The differences between these two conditions are addressed in a later section of this work.

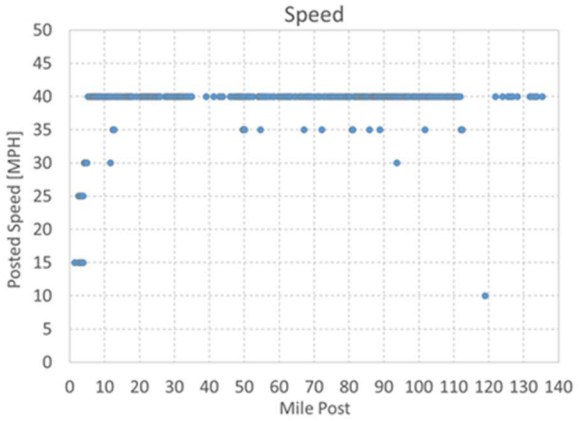

Figure 5. The posted train speed for curves vs. mile post for the subdivision.

The condition of the rail running surface is affected by cant deficiency and whether the track superelevation is adequate for the operating conditions. This has an influence on the amount of loading on the high rail where the rail failure took place. Understanding this relationship across the whole subdivision helped to determine the problem size.

To understand the track geometry condition on the line, NRC plotted the 'required' (based on speed shown in Figure 5) and 'actual' track superelevations vs. MP (see Figure 6).

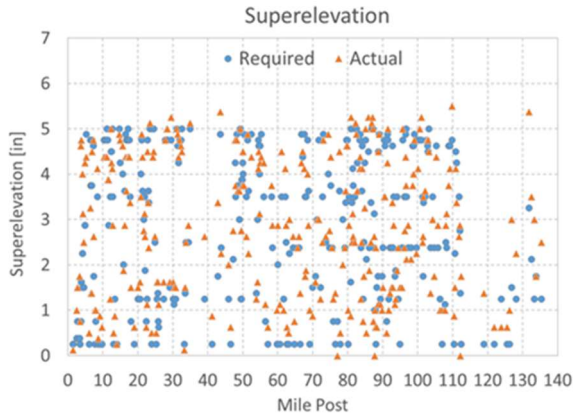

Figure 6. The 'required' and 'actual' track superelevation as a function of MP on the subdivision.

Both of these plots of superelevations vs. MP were essentially point clouds. However, mapping superelevation as a function of track curvature provided a much clearer understanding of its distribution in the subdivision (see Figure 7).

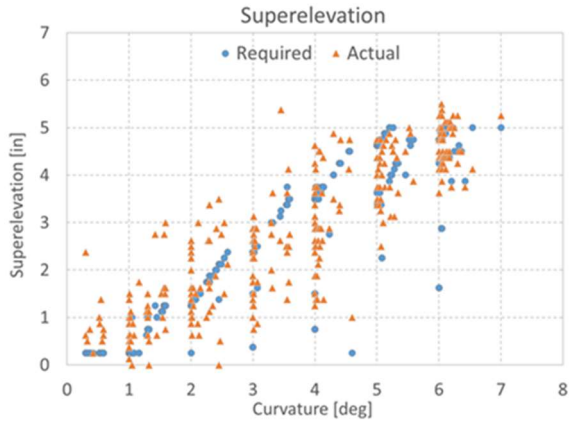

Figure 7. The 'required' and 'actual' track superelevation as a function of track curvature on the subdivision.

Seeing increasing superelevation with increasing curvature was a positive sign that superelevation was being matched to curvature to ensure balanced loading on the high and low rails at all times of train operation on the subdivision. However, as Figure 7 indicates, there was an observable difference between the designed (i.e. 'required') track superelevation and that present in track (i.e. 'actual'). This was an indication that the trend shown in Figure 7 was encouraging, but there were still many curves with incorrect elevation for the typical train speed.

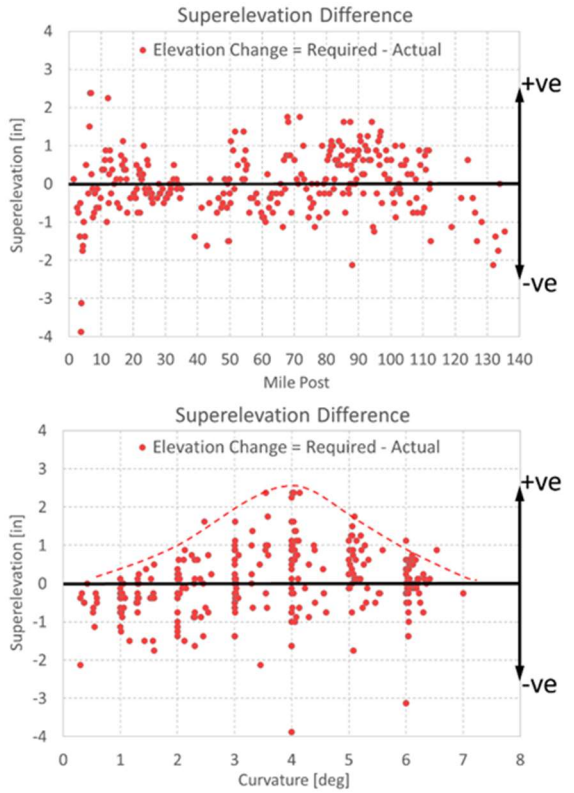

Figure 8. The elevation change (i.e. difference between required and actual superelevations) vs. MP and curvature on the subdivision.

Plotting the cant deficiency (i.e. the difference between the 'required' and 'actual' superelevations) across both MP and curvature (see Figure 8) revealed two things:

1. That superelevation difference varied up to ±2 inches across the entire subdivision.
2. That there appeared to be a normal distribution to the superelevation difference as a function of curvature for positive differences (i.e. when the high rail was overloaded due to insufficient curve elevation).

The physical significance of the positive and negative superelevation differences are best shown schematically.

At constant train speed in a constant-radius curve the overbalanced condition occurs when the loading on the low rail is elevated (or excessive). This results in excessive wear and plastic flow on the low rail. On the other hand, an underbalanced condition occurs when the loading on the high rail is elevated (or excessive). This results in excessive wear and plastic flow on the high rail. Neither of these conditions is desirable, as it shortens the overall life cycle of the track, as well as increases track maintenance costs.

The ideal condition is to have equal loading on both rails, as this distributes the wear and plastic flow evenly on both rails, thereby maximizing track longevity and reducing overall maintenance costs.

The differences between these three conditions are shown schematically in Figure 9.

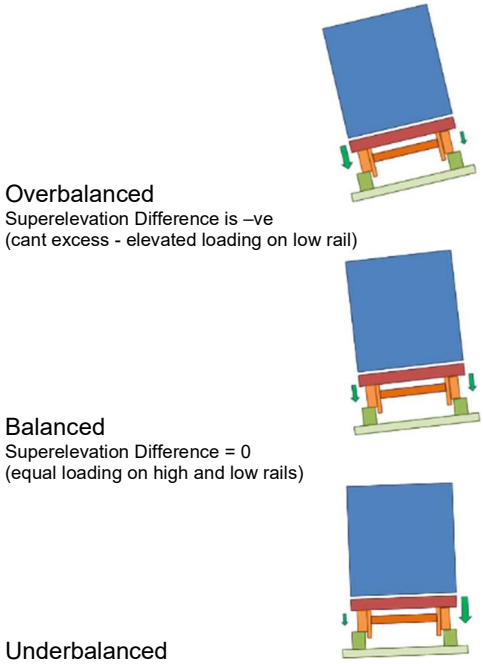

Figure 9. Schematic representation of the overbalanced, balanced, and underbalanced rail loading conditions due to superelevation differences in a curve. High rail is the right hand rail in each diagram.

Therefore a cant deficiency increases loading on the high rail, and this loading increases as the positive difference increases. Curves in the 3-5 degree range are the ones that had the greatest cant deficiency, and therefore suffered the greatest elevated loading on their high rails (see Figure 8).

NRC mapped out the cant deficiency as a function of MP to understand where the greatest density of cant-deficient curves were located on the subdivision. Based on this a 30 mile zone of track was selected for an on-site inspection.

A couple of indicators led to the selection of this 30 mile stretch of track:

1. It had the highest density of curves with cant deficiency (10+ curves where deficiency was greater than 1 inch). Assuming constant train speed, these were the curves where loading on the high rail would be the greatest (as compared to other curves on this subdivision), and therefore the risk of high rail fracture and subsequent train derailment would be most detrimental (assuming the surface damage on these rails was substantial).
2. The curvatures where these occur was in the 1-6 degree range, which was representative of the curve population on the subdivision.

Due to these two conditions the selected 30 mile section of track was deemed to represent the track zone of interest. A total of 29 curves were inspected on the subdivision during a two day visit.

The EC measurements for the RCF cracking at each location were graphed for both high and low rails as a function of track curvature (see two representative locations in Figure 10). These results indicate that maximum low rail cracking was approximately 3.5 mm in depth, whereas in the high rail its maximum depth was approximately 6.1 mm. In all locations, the crack depth on the high rail was greater than that on the low rail.

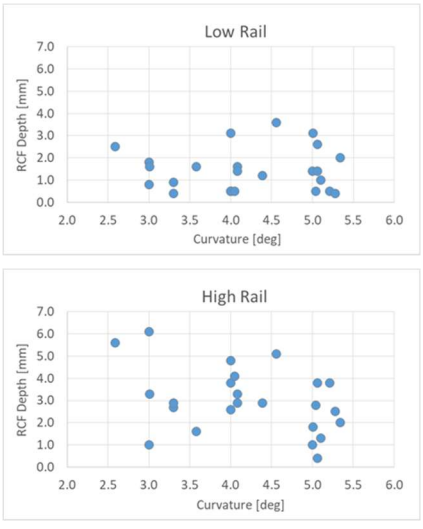

Figure 10. Eddy current RCF crack depth assessment in low and high rails as a function of track curvature in the 30 mile stretch of track.

Two representative locations were selected to show typical low and high rail damage observed in curves below 3 degrees of curvature, and in curves of 4 degree curvature and above. Results of these are shown in Figure 11.

2.59 degree curve

Low Rail | High Rail

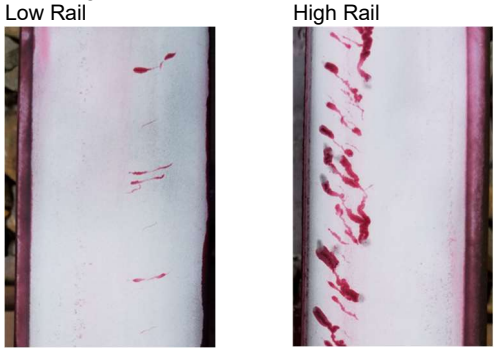

Existing Superelevation (track evaluation car): 2.125 in

RCF Cracks: 2.5mm deep | *RCF Cracks: 5.6mm deep*

Track Gauge: 1440.8mm
Grade: -0.6% (loaded train downhill)
Rail Type: Algoma 1985
Approximate Tonnage: 130MGT

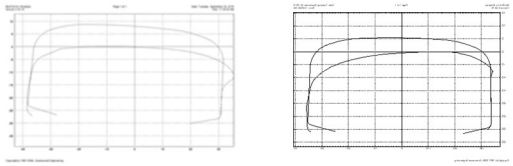

W1: 8.28mm
W2: -0.56mm
W3: 4.89mm

W1: 5.88mm
W2: 0.05mm
W3: 8.27mm

4.00 degree curve

Low Rail | High Rail

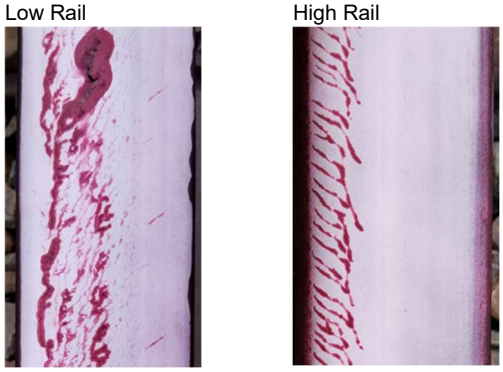

Existing Superelevation (track evaluation car): 3.625 in

RCF Cracks: 3.1mm deep | *RCF Cracks: 4.8mm deep*

Gauge: 1444.6mm
Grade: -1.2% (loaded train downhill)
Rail Type: Algoma 1985
Approximate Tonnage: 130MGT

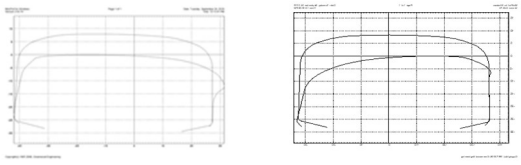

W1: 8.06mm
W2: -0.94mm
W3: 6.08mm

W1: 8.77mm
W2: 1.33mm
W3: 11.82mm

Figure 11. Select track inspection results for a 2.59 and 4.00 degree curvatures.

4 CONCLUSIONS

Two gauge corner fatigue cracks were found in the rail sections delivered to NRC for analysis. Only one of these cracks caused the rail break that led to a derailment. Both defects initiated at approximately the same geometric corner positions on the rail running surface (see Figure 1). They propagated to about the same cross-sectional size and then fractured critically causing multiple rail breaks. It is not possible to say which of these defects broke first. Once the rail broke at one location there would have been enough rail bending to cause a critical failure at the second location, hence the two breaks. However, only one of these defects would have caused the initial critical failure leading to derailment.

It is important to point out that both of the gauge corner fatigue cracks formed and grew in the high rail section independently, but through the same growth mechanism (i.e. metal fatigue due to load reversal that occurred during train travel over these defects). These defects formed over time as a result of inadequate rail grinding. As these defects were relatively deep compared to remaining rail cross-section the suggested course of action was rail replacement. It was also advised to replace any rails that displayed similar gauge corner fatigue defects in track.

Investigation of rail chemistry, microcleanliness and mechanical properties indicated that chemistry and microcleanliness for this 1985 rail grade were within the current AREMA recommended guidelines for standard rail type. Analysis of the mechanical properties indicated that yield strength (YS) and ultimate tensile strength (UTS) values were lower than recommended by the current AREMA guidelines for standard rail grade. These lower values mean the rails were more prone to plastic flow at the gauge corner (leading to earlier onset of fatigue cracking at that location) and critical rail failure (i.e. metal brittle failure at a lower stress) as compared to rails that meet all current AREMA guidelines for standard rail.

The suggested course of action going forward was to focus on more frequent defect inspections of the 1980s rails and prioritizing their replacement in the near future.

The main focus of the track inspection in the subdivision where the derailment took place was to investigate under-elevated curves since these locations would suffer premature high rail damage. Since only freight trains run on the investigated subdivision, changing the curve elevation to be balanced for the typical speed of loaded trains (which will cause more damage than empty trains) should be the main focus going forward.

Knowing the rail balanced loading condition is speed dependant, the first step should be an accurate mapping of the train speed profile in the subdivision. The next step would be to look at train lengths vs. curve and tangent lengths as the speed of loaded trains may change while the train is spanning two or three consecutive curves of different curvatures (i.e. affecting the balanced loading on each curve). This makes the selection of optimal superelevation difficult, since all above mentioned factors need to be taken into account simultaneously to yield the optimum solution.

To summarize, the following actions were suggested to be taken in this specified sequence:

- Review of subdivision track speed, grade for multiple train passes
- Review of track geometry (curve & tangent lengths) vs. train lengths in the track subdivision
- Review and adjustment of track elevation to fit the two conditions above

Besides adjusting track elevation, the focus should be on replacement of rails based on cracked depth vs. vertical or gauge face wear remaining on the high rail. Changing the elevation in curves with deep cracks and not much rail life remaining may not be as cost effective as just replacing the rail. If the cracks could be removed through rail grinding and the rail still had some wear life remaining, this might makes sense. This becomes an economic consideration, and effort should be placed on assigning resources adequately with that in mind.

Concerning rail replacement, premium or head hardened (HH) rails yield longer rail life as compared to standard or intermediate strength rail steels (nearly twice as much in a 5 degree curve location under heavy loading). This is due primarily to their resistance to plastic flow, and if the microstructural grain size is refined, to improved wear resistance. Use of the HH rails should be prioritized for higher degree curves, as these are most prone to premature wear problems (especially in an underbalanced curve condition).

In addition, the application of GF lubrication should also be improved to prevent the high rail lip formation due to plastic flow. Consistent GF lubrication will also improve rail wear performance, but will require periodic light grinding at roughly 60° to 70° on the gauge corner to prevent the formation of deep seated shells. Lack of lubrication causes the transverse rail profile to deteriorate more rapidly than it would with lubrication, which means it needs to be ground more frequently to maintain profile. Preventive grinding and good lubrication results in longer rail life than no lubrication and/or grinding.

TOR FM helps in extending rail life even further but the payback period on low tonnage lines makes its use unattractive due to cost of initial investment. For low tonnage lines this is true from a rail wear perspective. However, use of TOR FM might be useful from an RCF prevention point of view and in terms of increasing grinding interval due to reduced transverse profile deterioration. In either case, both arguments circle back to an economic consideration and whether the initial investment if offset by the payback period.

One of the drawbacks of this analysis was the lack of wheel profile information. During the visit we did not have access to vehicles to acquire wheel profiles (which could then be matched with the rail profiles to perform a W/R contact analysis and to establish its impact on RCF damage). There would be value in acquiring such

information in the future to make the site analysis more complete.

5 ACKNOWLEDGEMENT

The authors would like to express appreciation for the support of the railroad that supplied the rails for analysis and subsequent access to its track for the site investigation.
Special thanks to Alexandre Woelfle (NRC-AST) for contribution to information provided in Figure 9 as well as discussions concerning superelevation vs. rail loading conditions.

6 REFERENCES

Aquib Anis M., Srivastava J.P., Duhan N.R., Sarkar P.K. (2018), *Rolling contact fatigue and wear in rail steels: An overview*, IOP Conference Series: Materials Science and Engineering 377 012098.

AREMA, American Railway Engineering and Maintenance-of-Way Association (2021), Chapter 4 – Rail.

CPR, Canadian Pacific Railroad, *White Paper: Railroading in the Canadian Winter* (2019), https://www.cpr.ca/en/about-cp-site/Documents/CP-2018-19-WhitePaper.pdf

Harmon M., Lewis R., (2016), *Review of top of rail friction modifier tribology*, Tribology Materials, Surface and Interfaces, 10 (3).

Magel E., Kalousek J., Sroba P. (2014), *Chasing the magic wear rate*, Proceedings of the Second International Conference on Railway Technology: Research, Development and Maintenance.

Magel E., Mutton P., Ekberg A., Kapoor A. (2016), *Rolling contact fatigue, wear and broken rail derailments*, Wear, http://dx.doi.org/ 10.1016/j.wear.2016.06.009.

PTS & MTS, Physical Testing Standards and Mechanical Testing Standards (2021), ASTM, www.astm.org

Sroba P. (2003), *Rail Grinding Best Practice For Committee 4, Sub-Committee 9*, AREMA

Szablewski D., Kalay S., LoPresti J. (2011a), *Preliminary Evaluation of Premium Rail Steels for Heavy Haul Operations*, AAR Technology Digest, TD-11-031

Szablewski D., Kalay S., LoPresti J. (2011b), *Preliminary Evaluation of Intermediate Hardness Rails for Heavy Haul Operations*, AAR Technology Digest, TD-11-032

TSBC, Transportation Safety Board of Canada, Rail Transportation Occurrences in 2019, https://www.bst-tsb.gc.ca/eng/stats/rail/2019/sser-ssro-2019.html.

Tuzik B. (2019), *Getting a Grip on Friction Management*, RT&S, Track Maintenance.

Wang W.J., Lewis R., Evans M.D., Liu Q.Y. (2017), *Influence of Different Application of Lubricants on Wear and Pre-existing Rolling Contact Fatigue Cracks of Rail Materials*, Tribology Letters v. 65, article 58.